Lamellar to micelle transition of nonionic surfactant assemblies induced by addition of colloidal particles

Yukiko Suganuma,[1] Naohito Urakami,[2] Rina Mawatari,[1] Shigeyuki Komura,[3] Kaori Nakaya-Yaegashi,[1] and Masayuki Imai[1,a)]
[1]*Department of Physics, Faculty of Science, Ochanomizu University, Otsuka, Bunkyo, Tokyo 112-8610, Japan*
[2]*Department of Physics, Biology and Informatics, Yamaguchi University, Yoshida, Yamaguchi 753-8512, Japan*
[3]*Department of Chemistry, Graduate School of Science and Engineering, Tokyo Metropolitan University, Minami-Osawa, Hachioji, Tokyo 192-0397, Japan*

(Received 2 January 2008; accepted 14 August 2008; published online 7 October 2008)

We have investigated the entropic interactions between lamellar membranes and spherical colloidal particles using a small-angle neutron scattering (SANS) technique. By adding colloidal particles between lamellar sheets, the first lamellar peaks in SANS profiles become intense and the second and higher order Bragg peaks begin to appear, indicating that the membrane fluctuations are suppressed by the colloidal particles. We estimate the interlamellar interaction potential in the presence of the colloidal particles from the layer compressibility obtained by the SANS profile analysis and propose a phenomenological free energy model based on the restriction of membrane fluctuations. By further addition of the colloidal particles, the lamellar membranes transform to prolate micelles. In order to release the strong frustration due to the restriction of membrane fluctuations, the surfactant assemblies change the morphology from the two dimensional sheets to the one dimensional prolate micelles. © *2008 American Institute of Physics*.
[DOI: 10.1063/1.2978385]

I. INTRODUCTION

Nowadays complex systems consisting of various kinds of soft materials, such as polymers, colloidal particles, liquid crystals, and amphiphilic assemblies, have acquired great interests, because these complex materials are widely observed in biological systems and are extensively used in pharmaceutical, cosmetic, food, and other fine chemical products. By doping guest particles into a host mesoscopic structure (mesostructure) of soft matter, the dominant interactions that stabilize the mesostructure are modified by additional entropic interactions originated from the geometrical restriction. The most familiar entropic interaction is the depletion interaction,[1–3] which is an attractive interaction between the host colloidal particles. The depletion interaction was first recognized in the spherical colloid and polymer mixture systems and then observed in various soft matter complex systems, such as rod and sphere mixture systems.[1,4–12] In these systems, by overlapping the depletion zone around the host particles, the guest particles obtain large free volume. Increase of the free volume raises the translational entropy of guest particles but at the expense of lowering the entropy of mixing. If the gain in free volume is sufficient, the host particles aggregate, i.e., the attractive interaction between the host colloidal particles. This concept is easily extended to more complicated systems, such as membrane/polymer[13–17] and membrane/colloid[18–20] systems. The polymer doped lamellar membrane systems were investigated theoretically by Daoud and de Gennes,[13] and revisited by Brooks and Cates.[14] Their theoretical predictions were experimentally confirmed by Ligoure *et al.*[15–17] By doping neutral polymer chains between the lamellar sheets, the attractive interlamellar interaction is induced so as to obtain the large free volume for the guest polymer chains by overlapping the depletion zones of the adjacent membranes. This attractive interlamellar interaction (depletion interaction) destabilizes the lamellar membranes and finally causes a phase separation into a dilute lamellar phase where the polymer chains are localized in a concentrated lamellar phase.

On the other hand, the repulsive interlamellar interaction is induced by doping neutral colloidal particles without specific interactions with the membranes.[18,19] The repulsive interaction originates from the restriction of the lamellar fluctuations by the presence of the colloidal particles. The restriction causes strong frustration to the lamellar membranes and finally destroys the structure.[19]

On the basis of the above results, we systematically investigate the structural transition of lyotropic lamellar phase induced by the addition of colloidal particles. We use the nonionic surfactant lamellar system, where the interlamellar interactions are governed by the Helfrich interaction[21] and the structural changes of lamellar membranes induced by the addition of colloidal particles are followed by a small-angle neutron scattering (SANS) technique. The intermembrane interaction mediated by the presence of the colloidal particles is estimated from the layer compression modulus $\bar{B}$ obtained by the SANS profile analysis. In order to explain the effects of colloidal particles $\bar{B}$, we propose a phenomenological free

a)Author to whom correspondence should be addressed. Electronic mail: imai@phys.ocha.ac.jp.

energy model. Further addition of colloidal particles brings a morphology transition of the surfactant assembly. In order to determine the morphology of surfactant assemblies, we performed contrast matching experiments of SANS, where the interference between the scattered neutrons from membranes and colloidal particles can be neglected. We will discuss the morphology transition from entropic interactions induced by geometrical restrictions.

II. EXPERIMENTS

A. Samples

In this study we investigated ternary mixtures of water/$C_{12}E_5$/spherical colloidal particle. The nonionic surfactant $C_{12}E_5$ (purity $>98\%$) was purchased from Nikko Chemicals Inc. and used without further purification. The phase behavior of the $C_{12}E_5$/water system is well characterized and we can control the interlamellar distance by a simple dilution law.[22] As the spherical colloidal particles, we used the polystyrene latex purchased from Magsphere Inc. as a 10% suspension in H_2O. The purchased latex particles of radius $R_c=80$ Å have surface charge $\sim 0.1\ e/\mathrm{nm}^2$ but no steric layer covering colloid surface. In order to remove the excess surfactants and impurities, the latex solutions were dialyzed using cellulose tubes (Viskase Companies Inc, pore size 40–50 Å) against purified water for about two weeks. The completeness of the dialysis was verified by adsorption spectrum measurements in the region of 200–400 nm. We confirmed by the SANS profiles that the dialysis did not induce the aggregation of the colloidal particles.

In this study we performed two types of SANS experiments to make clear the structures of surfactant assemblies, one is a standard SANS measurement and the other is the contrast matching measurement. The standard SANS experiments for surfactant and colloid mixture systems were performed using D_2O/H_2O mixture solvent with the composition of 85/15, except for the sample with $\Phi_c=1.3\%$ (Φ_c: volume fraction of colloidal particles). For the mixtures with $\Phi_c=1.3\%$, we used the solvent with the composition of $D_2O/H_2O=48/52$. On the other hand, for the contrast matching experiments, the D_2O/H_2O mixture solvent had a matching composition of 28.5/71.5. Details of the contrast matching experiment will be described in a contrast matching technique of SANS section.

The ternary mixtures composed of water/$C_{12}E_5$/colloidal particle were prepared by the following procedure. The required amounts of surfactants ($C_{12}E_5$) were dissolved in colloidal suspensions with prescribed colloid concentrations and the mixtures were homogenized using a vortex mixer at room temperature (micellar phase). We increased the sample temperature (T) to the measurement temperature (57 °C: lamellar phase) and then equilibrated the sample for several minutes after the homogenization. During the scattering measurements at 57 °C, we regulated the temperature within ±0.1 °C of accuracy. In this study we prepared two series of samples. In the first series we fixed the volume fraction of surfactant to $\Phi_s=3.1\%$ and varied the volume fractions of colloidal particles in the range of $0\% < \Phi_c < 3.0\%$; on the other hand, in the second series, we fixed Φ_c to 0.01% and 0.02%, and varied Φ_s in the range of $3.1\% < \Phi_s < 8.3\%$. It should be noted that in both series the mean interlamellar distance $\bar{d}$ ($\bar{d}=d-\delta$, d: lamellar repeat distance and δ: membrane thickness) is fairly larger than the size of the colloidal particles. The samples in the lamellar phase without colloidal particles were monophasic and slightly cloudy; however, in the presence of the colloidal particles, the samples became transparent.

B. Instruments

SANS measurements were carried out using the SANS-U instrument of Institute of Solid State Physics, University of Tokyo at JRR3-M reactor of the Japan Atomic Energy Research Institute in Tokai.[23,24] In this experiment we used neutron beam having a wavelength (λ) of 7.0 Å with the resolution of $\Delta\lambda/\lambda=15\%$. The diameter of the irradiated neutron beam was 5 mm and the scattered neutrons were detected by a two dimensional (2D) position sensitive detector with the sample to detector distances of 1, 4, and 12 m, which covers q (magnitude of scattering vector, $q=4\pi \sin\theta/\lambda$, 2θ: scattering angle) range from 0.002 to 0.3 Å^{-1}. The two dimensional isotropic scattering patterns were corrected for heterogeneity of detector, background scattering, and the incoherent scattering intensity from the protonated substances. Then they were circularly averaged to obtain one dimensional scattering profiles. The calibration to the absolute intensity scale was performed using a standard sample of Lupolene.[24]

C. Contrast matching technique of SANS

Generally scattering function from the surfactant assembly and colloidal particle mixture is given by

$$I(q) = (\rho_c - \rho_w)^2 S_{cc}(q) + 2(\rho_c - \rho_w)(\rho_s - \rho_w) S_{cs}(q) + (\rho_s - \rho_w)^2 S_{ss}(q), \tag{1}$$

$$S_{ij}(q) = \int \langle \phi_i(\boldsymbol{r}_i)\phi_j(\boldsymbol{r}_j)\rangle \exp[-i\boldsymbol{q}\cdot(\boldsymbol{r}_i - \boldsymbol{r}_j)]d\boldsymbol{r}, \tag{2}$$

where ρ_i and $\phi_i(\boldsymbol{r})$ are the scattering length density and volume fraction of component i (i denotes the components c, s, and w for colloid, surfactant, and solvent, respectively). In order to obtain the scattering function from the surfactant assemblies without the interference effects, the scattering length density of the solvent is chosen to be the same as that of the colloidal particles. The contrast matching point was calculated by the following expression:

$$\rho_{D_2O} \times \phi_0 + \rho_{H_2O} \times (1 - \phi_0) = \rho_c, \tag{3}$$

where ϕ_0 is the volume fraction of D_2O in the solvent, and ρ_{D_2O} and ρ_{H_2O} are the scattering length densities of D_2O and H_2O, respectively. Using $\rho_{D_2O}=6.36\times10^{-6}$ Å^{-2}, $\rho_{H_2O}=-0.56\times10^{-6}$ Å^{-2}, and $\rho_c=1.41\times10^{-6}$ Å^{-2}, we obtained the D_2O volume fraction at the matching point as $\phi_0=0.285$. Actually the SANS profile of the colloidal suspension at the matching point showed no significant scattering from the colloidal particles. Under this matching condition, the scattering function is expressed by

$$I(q) = (\rho_s - \rho_w)^2 N_s P_s(q) S_s(q), \tag{4}$$

where N_s is the number density of the surfactant assemblies, and $P_s(q)$ and $S_s(q)$ are the form factor and the partial structure factor of the surfactant assembly.

III. DATA ANALYSIS

A. Estimation of intermembrane interaction

In order to estimate the intermembrane interaction potential, we extract the Caillé parameter η of fluctuating membranes from the SANS profiles. The Caillé parameter η (Ref. 25) is defined by

$$\eta = \frac{q_0^2 k_B T}{8\pi\sqrt{K\bar{B}}}, \tag{5}$$

where K is the bulk bending modulus ($K=\kappa/d$, where κ is the bending modulus for a single membrane) and q_0 is the position of the first Bragg peak. In the case of the lamellar phase containing guests, the layer compressibility $\bar{B}$ is related to the interlamellar interaction potential per unit bilayer area F_{l-l} by

$$\bar{B} = d\left\{ \frac{\partial^2 F_{l-l}}{\partial \bar{d}^2} - \frac{\left[\frac{1}{\bar{d}}\frac{\partial F_{l-l}}{\partial \bar{\Phi}_c} - \frac{\partial^2 F_{l-l}}{\partial \bar{\Phi}_c \partial \bar{d}}\right]^2}{\frac{\partial^2 F_{l-l}}{\partial \bar{\Phi}_c^2}} \right\}, \tag{6}$$

where $\bar{\Phi}_c$ is the volume fraction of the colloidal particles in water layers.[15,26] Thus, we can evaluate the interlamellar interaction potential from the compression modulus $\bar{B}$. In the previous paper, we showed by means of neutron spin echo measurements that the presence of the colloidal particles does not affect the bending modulus.[19] Then the modification of interlamellar interaction induced by the presence of colloidal particles can be evaluated through the Caillé parameter η. In the following, we explain the procedures to obtain η from the SANS profiles.

B. Analysis of SANS profiles of lamellar phase

The Caillé parameter η is a parameter to describe the correlation function of the fluctuating lamellar membranes and can be extracted from the static structure factor of the SANS function. Nallet *et al.*[27] proposed a model scattering function for the randomly oriented lamellar membrane system

$$I(q) = \frac{2\pi P(q) S(q)}{dq^2}, \tag{7}$$

with a form factor

$$P_{\text{neut}}(q) = \frac{2(\Delta\rho)^2}{q^2}[1 - \cos(q\delta_{\text{neut}})e^{-q^2\sigma^2/2}], \tag{8}$$

where δ_{neut} is the thickness of membrane determined by the SANS, σ is the measure of membrane thickness distribution fixed at $\delta_{\text{neut}}/4$, and $\Delta\rho$ is the scattering contrast between the membrane and the solvent. The structure factor $S(q)$ is given by

$$S(q) = 1 + 2\sum_{n=1}^{N-1}\left(1 - \frac{n}{N}\right)\cos\left(\frac{qdn}{1 + 2\Delta q^2 d^2 \chi(n)}\right) \times \exp\left[-\frac{2q_z^2 d^2 \alpha(n) + \Delta q^2 d^2 n}{2(1 + 2\Delta q^2 d^2 \chi(n))}\right]\frac{1}{\sqrt{1 + 2\Delta q^2 d^2 \chi(n)}}, \tag{9}$$

where N is the number of layers. The correlation function of fluctuating membranes $\chi(n)$ is given by

$$\chi(n) = \frac{\eta}{4\pi^2}[\ln(\pi n) + \gamma], \tag{10}$$

where γ is Euler's constant. The width of the resolution function is expressed by Δq and we adopted the following expression:

$$\Delta q^2 = q^2 \frac{1}{8\ln 2}\left(\frac{\Delta\lambda}{\lambda}\right)^2 + \frac{(2\pi)^2}{12\lambda^2}\left[3\frac{R_1^2}{L_1^2} + 3\frac{R_2^2}{L'^2} + \frac{(\Delta R)^2}{L_2^2}\right], \tag{11}$$

$$L' = \frac{L_1 L_2}{L_1 + L_2}, \tag{12}$$

where R_1 is the radius of the source aperture (10 mm), R_2 is the radius of the sample aperture (2.5 mm), L_1 is the incident flight path length, L_2 is the scattered flight path length, and ΔR is the detector resolution (5 mm).[28] For the data analysis, we used the isotropic 2D scattering patterns indicating randomly oriented lamellar systems.

IV. RESULTS AND DISCUSSIONS

A. Phase behavior of lamellar membrane and colloidal particle mixtures

In the previous paper,[19] we reported that the addition of the neutral polymer into the flexible lamellar membranes induces an attractive interlamellar interaction and finally destabilizes the lamellar phase. The attractive interaction can be interpreted by the depletion interaction for the membrane and polymer mixture systems. In contrast, the spherical colloidal particles confined between the lamellar membranes suppress lamellar fluctuations, which results in the effective repulsive interlamellar interaction. Figure 1(a) shows a series of SANS profiles as a function of volume fraction of the colloidal particle Φ_c at a constant volume fraction of the nonionic surfactant $C_{12}E_5$, Φ_s=3.1%. Here we shifted the SANS profiles vertically to avoid the overlapping of the profiles. The standard profile is the top profile in the figure and each profile is multiplied by a factor of 0.1. Without the colloidal particles, the scattering profile shows monotoni-

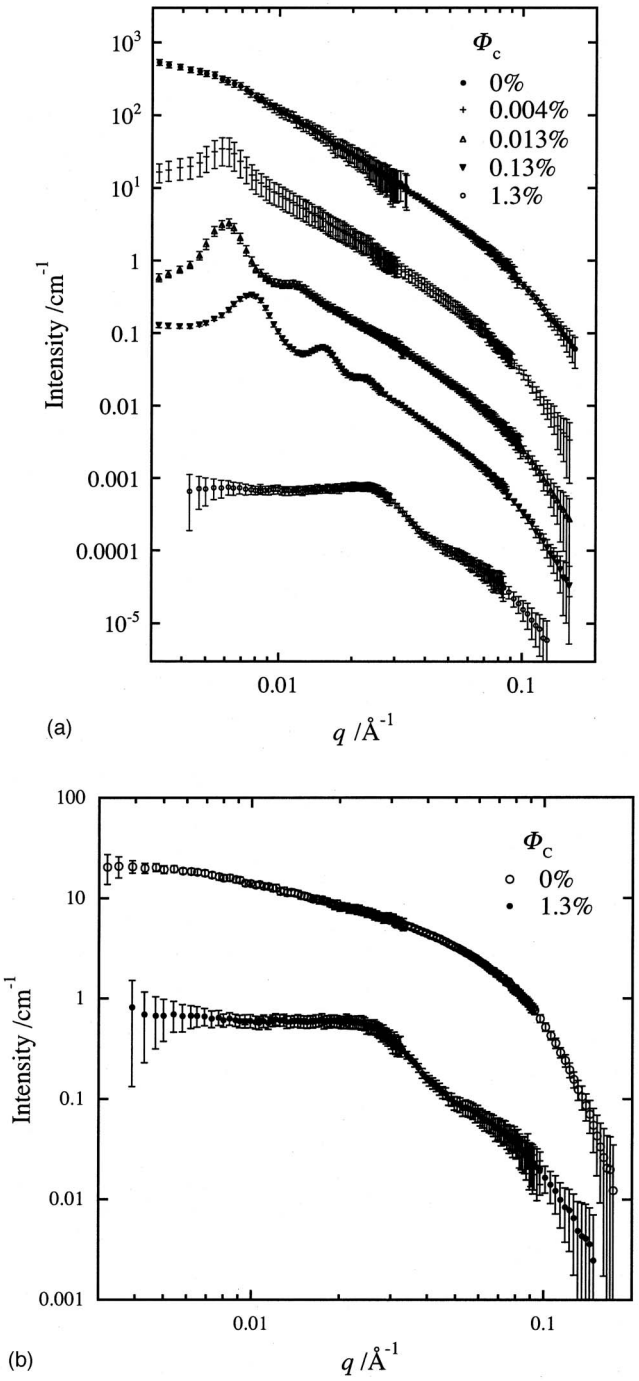

FIG. 1. (a) Change of SANS profiles by addition of colloidal particles into the lamellar phase as a function of Φ_c at constant $\Phi_s=3.1\%$ and $T=57\ ^\circ C$. For the mixtures with $0\% < \Phi_c < 0.13\%$, the solvent has the composition of $D_2O/H_2O=85/15$ and for the mixture with $\Phi_c=1.3\%$ the solvent has the composition of $D_2O/H_2O=48/52$. (b) Change of SANS profiles by addition of colloidal particles into the micellar phase at $16\ ^\circ C$ ($\Phi_s=3.1\%$, $\Phi_c=0.0\%$ in $D_2O/H_2O=85/15$ solvent and $\Phi_s=3.1\%$, $\Phi_c=1.3\%$ in $D_2O/H_2O=48/52$ solvent). For both figures, the standard profile is the top profile and each profile is multiplied by a factor of 0.1 to avoid overlapping.

cally decreasing profile having no characteristic lamellar peaks, which is due to the large membrane fluctuations. The addition of colloidal particles causes the emergence of the first Bragg peak. With an increase of Φ_c, the first Bragg peak becomes sharper and the second and higher order Bragg peaks begin to appear, indicating that the membrane fluctuations are suppressed by the colloidal particles. When Φ_c reaches $\sim 0.1\%$, the scattering peaks shift toward higher q side, indicating a phase separation. Further increase of Φ_c causes a drastic change of the scattering profile at $\Phi_c \sim 1.3\%$, as shown in Fig. 1(a). The Bragg peaks characteristics of the lamellar phase disappear and the scattering profile in low q region becomes almost flat.

In Fig. 1(b) we show the change of SANS profiles by the addition of colloidal particles into the micellar phase at $16\ ^\circ C$ ($\Phi_s=3.1\%$, $\Phi_c=0.0\%$ in $D_2O/H_2O=85/15$ solution and $\Phi_s=3.1\%$, $\Phi_c=1.3\%$ in $D_2O/H_2O=48/52$ solution). The scattering profile of pure $C_{12}E_5$ micellar solution at $16\ ^\circ C$ is well described by the prolate core-shell model as shown later. By the addition of colloidal particles into the micellar phase, the scattering profiles are modified. The SANS profile for micelle+colloid system is very close to that obtained by the addition of colloidal particles into the lamellar phase shown in Fig. 1(a). These profiles suggest that the lamellar assembly is transformed to micellar structure by the doping of the colloidal particles.

We show the phase diagrams of the $C_{12}E_5$ and colloidal particle mixture system determined by eye observation in Fig. 2, (a) $\Phi_c - T$ phase diagram at $\Phi_s=3.1\%$ and (b) $\Phi_c - \Phi_s$ phase diagram at $T=57\ ^\circ C$. In the figures, open circles, crosses, and filled circles indicate lamellar phase (L_α), coexisting phase (L_α/L_1), and micellar phase (L_1), respectively. In order to construct these phase diagrams, we needed to equilibrate the samples for several days.[15] The $\Phi_c - T$ phase diagram indicates that with the increase of Φ_c, the micellar phase expands to higher temperature region, and accordingly the lamellar phase disappears. This phase behavior is consistent with the $\Phi_c - \Phi_s$ phase diagram, Fig. 2(b). Thus SANS profile change shown in Fig. 1(a) corresponds to the lamellar to micellar phase transition via the coexistence region.

Here we mention the nature of colloidal particles in the $C_{12}E_5$/water system. When we added a very small number of colloidal particles ($\sim 0.004\%$) into the dilute lamellar phase ($\Phi_s=3.1\%$), the SANS profiles showed a lamellar peak, as shown in Fig. 1(a), indicating suppression of lamellar membrane fluctuations. Whereas when we added the same number of colloidal particles into the micellar phase, the scattering profiles did not show any change [not shown in Fig. 1(b)], indicating that the micelle structure and intermicellar interaction are not affected by the addition of this very small number of colloidal particles. Thus the observed suppression of lamellar membrane fluctuations is caused by the geometry of surfactant assemblies and not by the specific interaction between the colloids and the surfactants. Next we consider whether the colloidal particles are confined between the lamellar sheets or not. As shown in Figs. 2(a) and 2(b), when we added a small number of colloids to the lamellar phase, the system kept the homogeneous one phase appearance, indicating that the colloidal particles are homogeneously distributed in the sample. In the one phase region, the SANS profiles of lamellar membrane and colloid mixture [Fig. 1(a)] showed that the lamellar peak position keeps constant

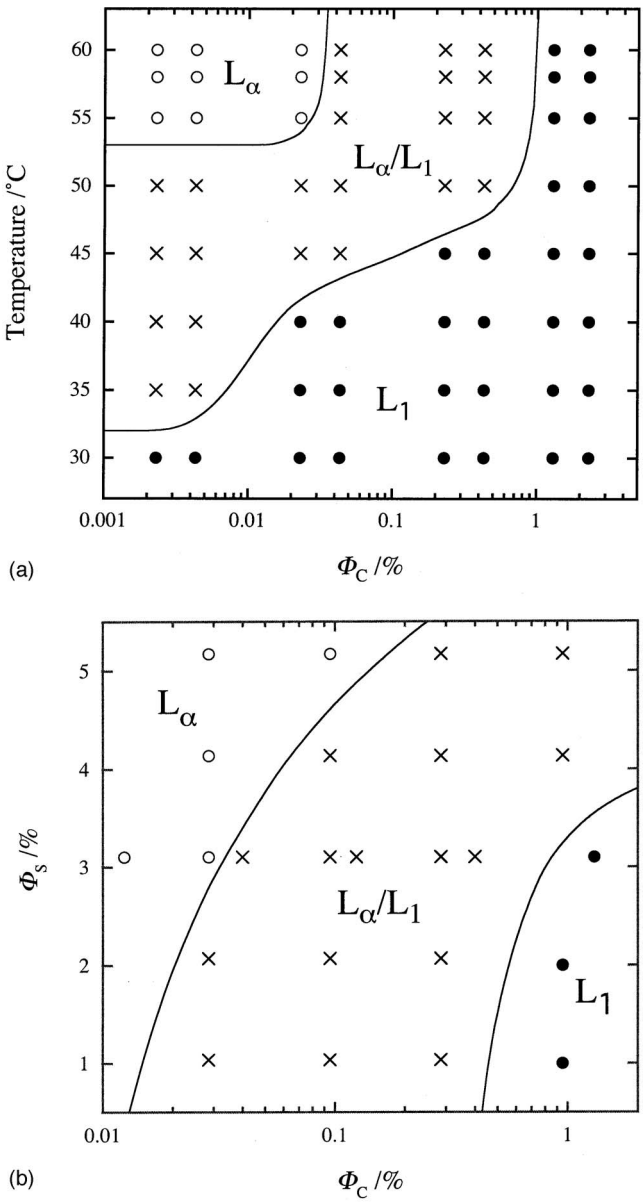

FIG. 2. Phase diagrams of $C_{12}E_5$+colloidal particle mixture system; (a) $\Phi_c - T$ phase diagram at $\Phi_s = 3.1\%$ and (b) $\Phi_c - \Phi_s$ phase diagram at $T = 57\,^\circ C$. For both figures, open circles, crosses, and filled circles indicate lamellar phase (L_α), coexisting phase (L_α/L_1), and micellar phase (L_1), respectively.

against Φ_c. These results are strong evidences for the confinement of colloidal particles between the lamellar membranes.

B. Interlamellar interactions mediated by addition of colloidal particles

When we confine a small amount of colloidal particles between the lamellar sheets, the scattering functions from the lamellar structure show the characteristic changes. In Fig. 3(a) we show detailed scattering profile change as a function of Φ_c at $\Phi_s = 3.1\%$. The addition of colloidal particles causes the sharpening of the first Bragg peak and the emergence of the second and higher order Bragg peaks. It is noteworthy that a very small number of the colloidal particles $\Phi_c \sim 0.003\%$ brings the change of scattering profile. On the other hand, when we increase Φ_s while keeping $\Phi_c = 0.01\%$, the lamellar peak position shifts toward high q side with decreasing peak intensity, as shown in Fig. 3(b). Thus the regularity of lamellar membranes decreases with decreasing the interlamellar distance. This is quite different from the behavior of pure nonionic surfactant/water systems. In the case of the pure nonionic surfactant/water systems, the amplitude of membrane fluctuations increases with increasing interlamellar distance, which makes the lamellar peak obscure. These results indicate that the confined colloidal particles modify the original interlamellar interaction (Helfrich interaction).

The mediated interlamellar interaction is examined through the layer compression modulus, which can be calculated from the Caillé parameter η and the bending modulus κ, as expressed in Eq. (5). The Caillé parameter was obtained by fitting of the observed SANS profiles with the model scattering function for lamellar membranes described in Sec. III. In Fig. 3(a) we show the results of fitting by the solid lines and the extracted parameters are tabulated in Table I. Here for pure lamellar structure ($\Phi_s = 3.1\%$) in the absence of colloidal particles, we show a predicted profile assuming that the interlamellar interaction is governed by the Helfrich interaction.[29]

The variation of obtained η as a function of Φ_c is plotted in Fig. 4(a). The Caillé parameter decreases monotonically with an increase of Φ_c, indicating the membrane fluctuations are suppressed by the colloidal particles. In order to obtain the layer compression modulus $\bar{B}$ from η, we have to estimate the value of the bending modulus κ. In the previous paper, we estimated the bending modulus from the dynamical structure factor of fluctuating membranes obtained by neutron spin echo measurements.[19] Using the values of η and κ, we calculated the layer compression modulus $\bar{B}$, as a function of Φ_c, as shown in Fig. 5(a). The layer compression modulus $\bar{B}$ increases with an increase of Φ_c in the range of $0.002\% < \Phi_c < 0.02\%$. Thus the addition of hard sphere colloids brings strong repulsive force between the adjacent lamellar membranes.

On the other hand, the scattering profiles from the dilute lamellar phase showed a characteristic Φ_s dependence, as shown in Fig. 3(b). In order to elucidate the characteristic behavior, we extracted the Caillé parameters from the SANS profiles. The results of fitting are shown by the solid lines in Fig. 3(b) and the obtained parameters are tabulated in Table I. The obtained Caillé parameters at $\Phi_c = 0.01\%$ and 0.02% are plotted as a function of interlamellar distance $\bar{d}$ in Fig. 4(b). The Caillé parameter decreases monotonically with increasing $\bar{d}$ for the both cases. When the interlamellar interaction is governed by the Helfrich interaction, the Caillé parameter is expressed by

$$\eta = 2\pi\sqrt{\frac{\mu}{3}}\left(1 - \frac{\delta_{\mathrm{Hel}}}{d}\right)^2 = 2\pi\sqrt{\frac{\mu}{3}}\left(\frac{\bar{d}}{d}\right)^2, \tag{13}$$

where δ_{Hel} is the effective membrane thickness based on the steric hindrance and μ is related to the local displacement of membranes $u(r)$ by the following geometrical expression:

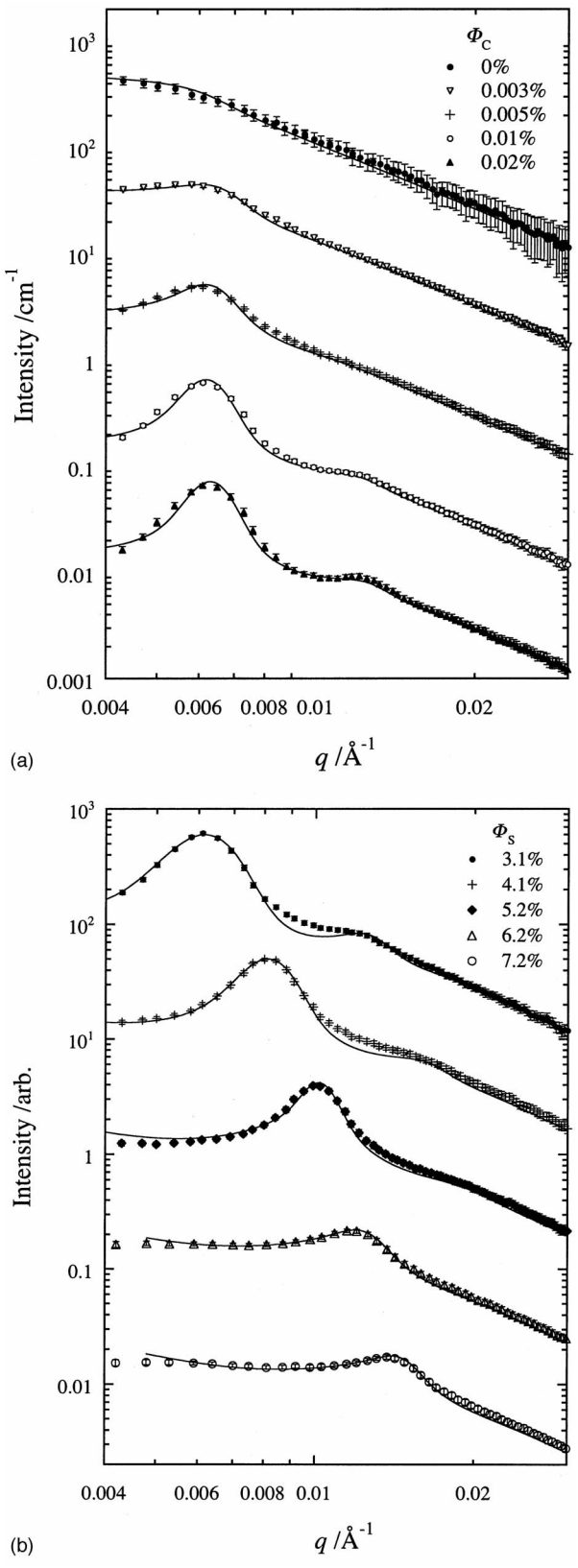

FIG. 3. A series of SANS profiles of lamellar membrane+colloidal particle mixture system as a function of Φ_c at Φ_s=3.1% (a) and Φ_s at Φ_c=0.01% (b). Both measurements were performed at 57 °C. For both figures, the solid lines indicate the results of fitting using model scattering function proposed by Nallet *et al.* For pure lamellar structure (Φ_s=3.1%) in the absence of colloidal particles, we show a predicted profile assuming that the interlamellar interaction is governed by the Helfrich interaction. For both figures, the standard profile is the top profile and each profile is multiplied by a factor of 0.1 to avoid overlapping.

TABLE I. Obtained parameters by fitting of SANS profiles of lamellar membrane+colloid systems.

Φ_s/%	Φ_c/%	d/Å	η
3.1	0.002	995	1.01
3.1	0.003	946	1.17
3.1	0.004	1003	0.85
3.1	0.005	979	0.82
3.1	0.006	1004	0.63
3.1	0.007	980	0.68
3.1	0.008	1014	0.54
3.1	0.010	992	0.51
3.1	0.010	1006	0.52
3.1	0.012	997	0.50
3.1	0.014	974	0.50
3.1	0.019	975	0.46
4.1	0.010	755	0.50
4.1	0.020	760	0.43
5.2	0.010	573	0.63
5.2	0.020	593	0.49
6.2	0.010	499	0.63
6.2	0.020	507	0.61
7.2	0.010	424	1.01
7.2	0.020	432	0.72

$$\langle u^2(r)\rangle = \mu \bar{d}^2. \tag{14}$$

In the previous paper we confirmed that the pure $C_{12}E_5$/water system satisfies the simple relation expressed by Eq. (13), which gives the values of μ=0.284 and δ_{Hel}=36 Å.[29] Thus, Caillé parameter increases with increasing $\bar{d}$, which is in contrast to the experimental results. By combining the bending modulus κ and the Caillé parameter η, we obtained the $\bar{d}$ dependence of the layer compression modulus at Φ_c=0.01% and 0.02%, as shown in Fig. 5(b). When the lamellar membranes confine colloidal particles, $\bar{B}$ decreases with an increase of $\bar{d}$.

The interlamellar interaction in the presence of colloidal particles shows two characteristic behaviors, $\bar{B}$ increases with an increase of Φ_c and decreases with an increase of $\bar{d}$. To describe these behaviors, we already proposed a model in which the colloidal particles suppress the fluctuations of membranes.[19,30] Following the Helfrich formulation,[21] the free energy of the interlamellar interaction in the presence of colloidal particles per unit area of the membrane is given by

$$F_{l-c} = \frac{(k_B T)^2}{32\mu\kappa} \frac{1}{\bar{d}^2 \tanh^n\left(\frac{1}{w\bar{\Phi}_c^{\mathrm{eff}}}\right)}, \tag{15}$$

where n and w are the constants describing the degree of suppression of membrane fluctuations by the colloidal particles.[30] In this expression we introduced a phenomenological volume fraction of colloidal particles between lamellar sheets $\bar{\Phi}_c^{\mathrm{eff}}$ given by

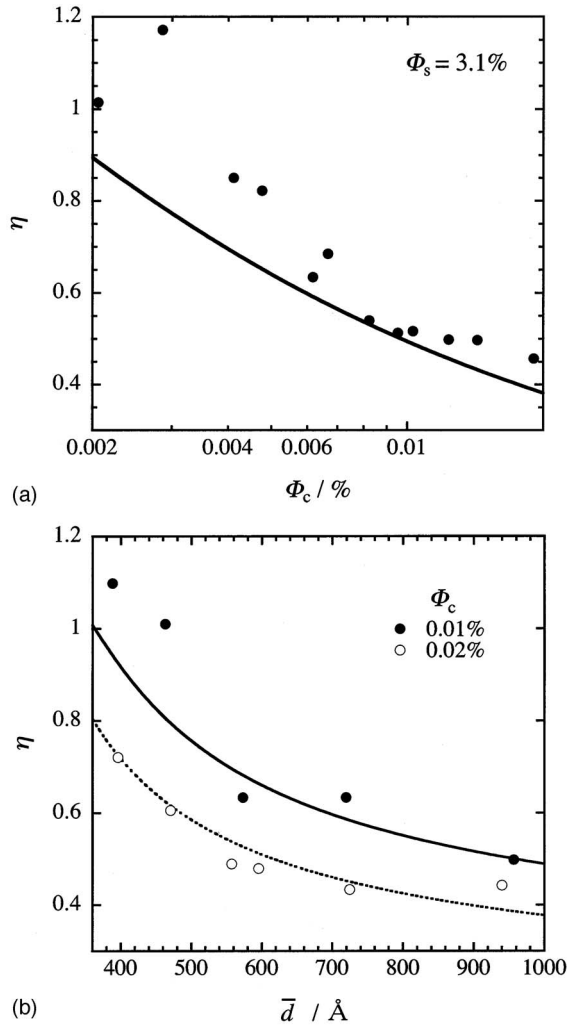

FIG. 4. Caillé parameters η of lamellar membrane+colloidal particle mixture. (a) Φ_c dependence at Φ_s=3.1% with theoretical prediction based on Eq. (20) indicated by the solid line and (b) $\bar{d}$ dependence at Φ_c=0.01% and 0.02% with theoretical predictions based on Eq. (20) indicated by the solid line for Φ_c=0.01% and the dotted line for Φ_c=0.02%.

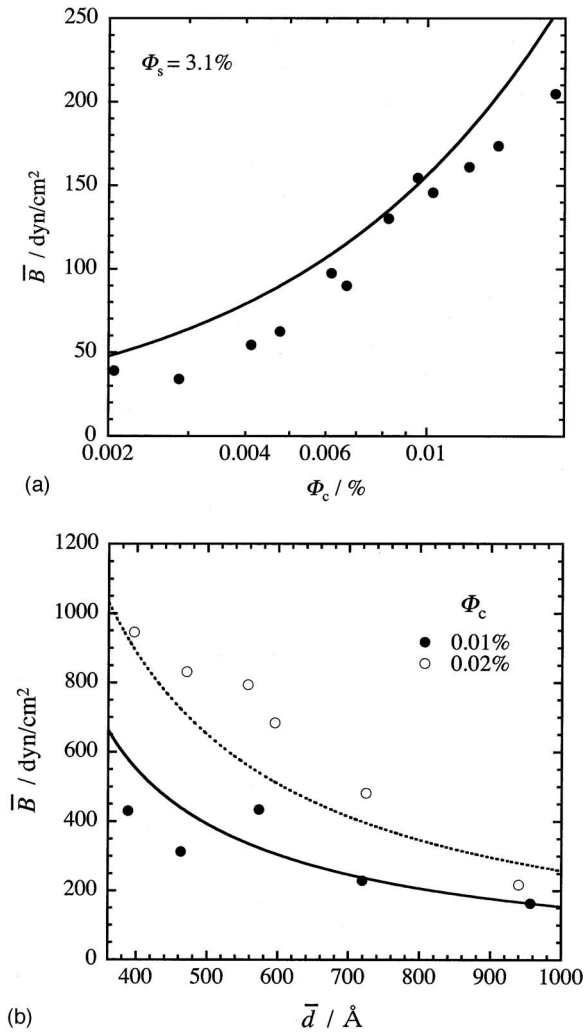

FIG. 5. Layer compression modulus $\bar{B}$ of lamellar membrane+colloidal particle mixture. (a) Φ_c dependence at Φ_s=3.1% with theoretical prediction based on Eq. (17) indicated by the solid line and (b) $\bar{d}$ dependence at Φ_c =0.01% and 0.02% with theoretical predictions based on Eq. (17) indicated by the solid line for Φ_c=0.01% and the dotted line for Φ_c=0.02%.

$$\bar{\Phi}_c^{\text{eff}} = \bar{\Phi}_c \left(\frac{\bar{d}}{R_c} \right)^m, \tag{16}$$

where the exponent m is an unknown parameter and should be determined by the comparison with experimental results. The layer compression modulus for the lamellar membranes confining colloidal particles can be calculated using Eqs. (6) and (15) as

$$\bar{B}_{l-c} = \frac{d}{32\mu} \frac{(k_B T)^2}{\kappa \bar{d}^4} \frac{g(\bar{\Phi}_c^{\text{eff}})}{h(\bar{\Phi}_c^{\text{eff}})}, \tag{17}$$

$$g(\bar{\Phi}_c^{\text{eff}}) = -3\bar{d}^2\bar{\Phi}_c^2 - 2mn^2\left(\frac{R_c^m}{w}\right)^2 + 2m^2n^2\left(\frac{R_c^m}{w}\right) + 2(m-1)mn\frac{2R_c^m}{w}\cosh\left(\frac{2}{w\bar{\Phi}_c^{\text{eff}}}\right) + n\left(\frac{R_c^m}{w}\right)\bar{d}^m\bar{\Phi}_c \sinh\left(\frac{2}{w\bar{\Phi}_c^{\text{eff}}}\right)(3-4m-m^2) - 3\left(\frac{R_c^m}{w}\right)\bar{d}^m\bar{\Phi}_c \sinh\left(\frac{4}{w\bar{\Phi}_c^{\text{eff}}}\right) + 3\bar{d}^{2m}\bar{\Phi}_c^2 \cosh\left(\frac{4}{w\bar{\Phi}_c^{\text{eff}}}\right), \tag{18}$$

$$h(\bar{\Phi}_c^{\text{eff}}) = 2\bar{d}^m\bar{\Phi}_c \sinh\left(\frac{1}{w\bar{\Phi}_c^{\text{eff}}}\right)\cosh\left(\frac{1}{w\bar{\Phi}_c^{\text{eff}}}\right) \times \tanh^{-n}\left(\frac{1}{w\bar{\Phi}_c^{\text{eff}}}\right)\left[-n\left(\frac{R_c^m}{w}\right) - \left(\frac{R_c^m}{w}\right)\cosh\left(\frac{2}{w\bar{\Phi}_c^{\text{eff}}}\right) + \bar{d}^m\bar{\Phi}_c \sinh\left(\frac{2}{w\bar{\Phi}_c^{\text{eff}}}\right)\right]. \tag{19}$$

By substituting Eqs. (17)–(19) to Eq. (5), the Caillé parameter for lamellar membrane and colloid mixture, η_{l-c} is expressed by

$$\eta_{l-c} = 2\pi\sqrt{2\mu}\left(\frac{\bar{d}}{d}\right)^2 \sqrt{\frac{h(\bar{\Phi}_c^{\text{eff}})}{g(\bar{\Phi}_c^{\text{eff}})}}. \tag{20}$$

In Figs. 4(a) and 4(b) we show the experimentally obtained $\bar{\Phi}_c$ and $\bar{d}$ dependences of η with the fitting results using Eq. (20), respectively. In both cases our model describes the observed data using the numerical parameters of $m=2.3$, $n=0.75$, and $w=1200$. Furthermore we calculated the layer compression modulus $\bar{B}$ using Eq. (17) with the same numerical parameters. The theoretical predictions of $\bar{\Phi}_c$ and $\bar{d}$ dependences of $\bar{B}_{l-c}$ agree with the experimentally obtained $\bar{B}$ behaviors, as shown in Figs. 5(a) and 5(b). Thus we consider that our free energy model is suitable to describe the interlamellar interaction in the presence of colloidal particles. By confining the colloidal particles between the lamellar sheets, the particles suppress the membrane fluctuations due to the steric hindrance, which brings entropic repulsive interaction.

C. Morphology transition of surfactant assembly induced by addition of colloidal particles

Further addition of colloidal particles brings the lamellar to micellar transition. In order to confirm the lamellar to micelle transition, we performed the contrast matching SANS measurements for pure micelle phase ($\Phi_s=3.1\%$) at $T=16$ °C, the micelle plus the colloidal particle mixture ($\Phi_s=3.1\%$ and $\Phi_c=1.3\%$) at $T=16$ °C and the lamellar membrane plus the colloidal particle mixture ($\Phi_s=3.1\%$ and $\Phi_c=1.3\%$) at $T=57$ °C. The obtained scattering profiles are shown in Fig. 6. We fitted the observed scattering profiles using the scattering function for prolate core-shell model[31,32] given by

$$I(q) = N_m \int g(r) P_m(q,r) dr S'_m(q), \tag{21}$$

where N_m is the number density of micelles. For the form factor $P_m(q)$, we adopted a prolate core-shell model expressed by

$$\langle P_m(q)\rangle \equiv \int_0^1 |H(q,x)|^2 dx, \tag{22}$$

$$H(q,x) = (\rho_t - \rho_h)\frac{4}{3}\pi a_t R_t^3\left[3\frac{j(u_t)}{u_t}\right] + (b_h - b_s)\frac{4}{3}\pi a R^3\left[3\frac{j(u)}{u}\right], \tag{23}$$

$$u_t = qR_t\sqrt{a_t^2x^2 + (1-x^2)}, \quad u = qR\sqrt{a^2x^2 + (1-x^2)}. \tag{24}$$

Here, R and R_t, are the outer and inner radii of the prolate minor axis, a and a_t are the ratios of major to minor axes for the outer and inner radii, respectively, and $j(x)$ is the first-order spherical Bessel function. The scattering length densities b_t, b_k, and b_s correspond to the hydrophobic, the hydrophilic, and the solvent regions, respectively. The apparent

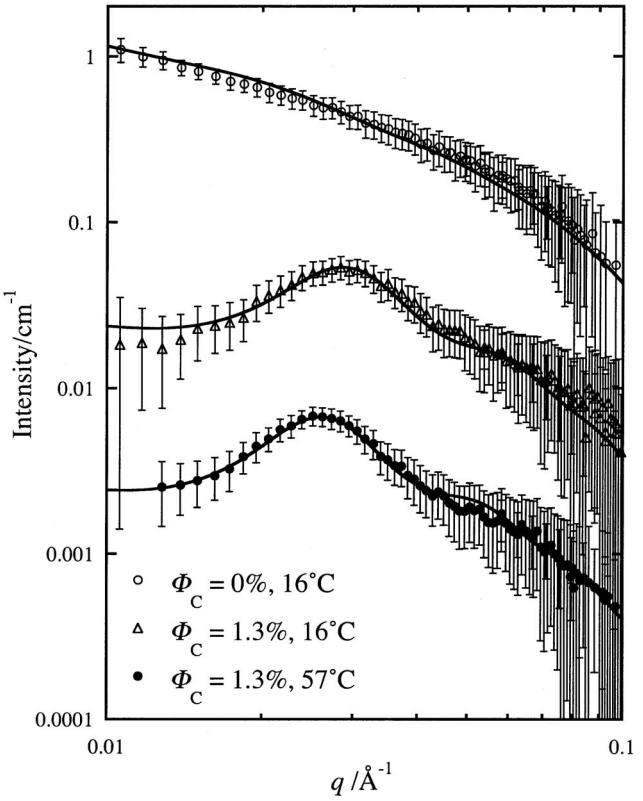

FIG. 6. SANS profiles for pure micellar phase ($\Phi_s=3.1\%$ and $T=16$ °C) and the $C_{12}E_5$+colloidal particle mixture ($\Phi_s=3.1\%$ and $\Phi_c=1.3\%$) at $T=16$ and 57 °C at contrast matching condition. The solid lines indicate the results of fitting using prolate core-shell model. In the figure, the standard profile is a top profile and each profile is multiplied by factor of 0.1 to avoid overlapping.

structure factor $S'_m(q)$ (Refs. 31 and 32) is related to the true structure factor $S_m(q)$ by

$$S'_m(q) = 1 + \beta(q)[S_m(q) - 1], \tag{25}$$

$$\beta(q) = |\langle H(q)\rangle|^2/\langle|H(q)|^2\rangle. \tag{26}$$

The true structure factor $S(q)$ for prolate micelles was calculated by assuming that a prolate micelle can be treated as a rigid sphere having equivalent volume. The polydispersity of micelle core radius is expressed by the Gaussian distribution function $g(r)$ in Eq. (21),

$$g(r) = \frac{1}{\sqrt{2\pi\nu}}\exp[-(r-R_t^m)^2/2\nu^2], \tag{27}$$

where ν is the variance and R_t^m is the mean micelle inner radius of the prolate minor axis.

Using the hard core intermicellar interaction potential (Percus–Yevick approximation[33]), we fitted the observed scattering function at the matching point and the result of fitting is shown in Fig. 6 by solid lines. The scattering profile of pure $C_{12}E_5$ micellar solution without colloidal particles at 16 °C ($\Phi_s=3.1\%$, $\Phi_c=0.0\%$) was well described by the model scattering functions with the fitting parameters of effective volume fraction of micelles $\Phi_{\text{mic}}^{\text{eff}}=5\%$, $R=28$ Å, $R_t^m=17$ Å, $a=18$ (micelle aggregation number, $N_{\text{agg}}=2730$), $b_t=-4.72\times10^{-6}$ Å^{-2}, $b_h=1.0\times10^{-7}$ Å^{-2}, $b_w=1.41\times10^{-6}$ Å^{-2},

ν=2.6 Å, and $N_m=1.4\times10^{15}$ micelles. Although the thicknesses of the hydrophobic part and hydrophilic part are consistent with the molecular structure, we found a very large axis ratio a=18 corresponding to the total micelle length of $L\sim1000$ Å. This long rod length is beyond the Kuhn length of the $C_{12}E_5$ micelle of ~200 Å.[34] Thus the micelles may have a semiflexible rodlike shape or a banana shape, which is consistent with the transmission electron microscopy observation of the $C_{12}E_5$ micelles[35] and the hydrodynamic radius of $C_{12}E_5$ micelles obtained by dynamical light scattering.[34] The large polydispersity of micelle radius (ν/R_t^m=0.15) obtained by the fitting may be due to the semiflexible nature.

By the addition of a small amount of colloid in the micelle phase, the scattering profile showed a characteristic broad peak even at low colloid volume fraction, Φ_c=1.3%. The fitting of the SANS profile gives the geometrical parameters of $\Phi_{\rm mic}^{\rm eff}$=26%, R=28 Å, R_t^m=17 Å, a=12, and $N_{\rm agg}$=1830. Thus by the addition of colloidal particles, the length of prolate micelle decreases. This observation is consistent with our previous reports.[36] We interpret the observed decrease of the prolate micelle length induced by the addition of colloidal particles using the depletion concept.[1–3,37] It is well known that in a colloid and polymer mixture, the centers of mass of polymer chains cannot approach closer than the radius of gyration of polymer chain from colloid surface, i.e., excluded volume called depletion zone. We applied this depletion concept to the colloid+elongated micelle system. The centers of mass of the semiflexible prolate micelle are excluded from "depletion zone" surrounding the surface of a colloidal particle. Then, in order to increase the free volume of micelles, the size of micelles may be decreased, which is consistent with our experimental results. It should be noted that the surfactant assembly has an ability to change its size depending on the external conditions.

In addition we observed large effective volume fraction, $\Phi_{\rm mic}^{\rm eff}$=26%, estimated by the fitting of the scattering profile. In this fitting we assumed that 6.6 water molecules hydrate one ethylene oxide group of the hydrophilic chains, which results in the scattering length density of $b_h=1.0\times10^{-7}$ Å^{-2}. This hydration of the hydrophilic chain gives the volume fraction of prolate micelles, $\Phi_{\rm mic}$=7.6% (Φ_s=3.1%), which is still smaller than the effective volume fraction of $\Phi_{\rm mic}^{\rm eff}$=26%. Then we applied the depletion concept. According to the depletion concept, the centers of mass of micelles cannot penetrate into the depletion zone, which increases the effective volume fraction of micelles. The contribution of the depletion zone to the effective volume fraction is expressed by a free volume fraction given by

$$\alpha = V_{\rm free}/V, \tag{28}$$

where V is the system volume and $V_{\rm free}$ is the free volume available for the micelles in the system. For the sake of simplicity, we regard a flexible prolate micelle as a spherical coil with a radius $R_m^{\rm eff}$ of 320 Å and estimate the free volume fraction using a scaled particle theory[38] expressed by

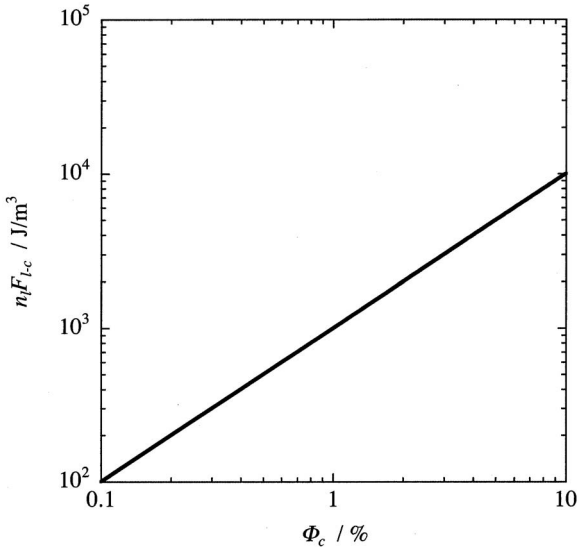

FIG. 7. Interlamellar interaction free energy in the presence of colloidal particles per unit volume as a function of Φ_c.

$$\alpha = (1-\Phi_c)\exp\left[-A_1\left(\frac{\Phi_c}{1-\Phi_c}\right)-A_2\left(\frac{\Phi_c}{1-\Phi_c}\right)^2 - A_3\left(\frac{\Phi_c}{1-\Phi_c}\right)^3\right], \tag{29}$$

with

$$A_1 = 3\xi + 3\xi^2 + \xi^3, \tag{30}$$

$$A_2 = 4.5\xi^2 + 3\xi^3, \tag{31}$$

$$A_3 = 3\xi^3, \tag{32}$$

where $\xi=R_{\rm m}^{\rm eff}/R_c$=4.0. Using this expression, we obtained α=0.276, which gives $\Phi_{\rm mic}$=0.275. This value is close to the effective volume fraction of $\Phi_{\rm mic}^{\rm eff}$=0.26. Then we consider that the large effective volume fraction is due to the depletion zone surrounding each colloidal particle.

When we add the colloidal particles into the lamellar phase (Φ_s=3.1%, Φ_c=1.3%, and T=57 °C), the scattering profile changes to the characteristic profile for the micellar phase with colloidal particles, as shown in Fig. 6. The fitting of obtained profile using the prolate core-shell model gave the following parameters of $\Phi_{\rm mic}^{\rm eff}$=0.28, R=28 Å, R_t^m=17 Å, a=14.8, and $N_{\rm agg}\sim2240$. Thus the length of the prolate micelle increases with the increase of temperature. In the case of nonionic surfactant/water systems, the length of elongated micelles increases with the increase of temperature,[39] which is consistent with our observation. Thus the observed scattering profiles show that by the addition of colloidal particles into the lamellar phase, the lamellar membranes transform to the prolate micelles.

Finally, we consider a scenario of the lamellar to micellar transition induced by the addition of colloidal particles. In Fig. 7 we plot the interlamellar interaction free energy in the presence of colloidal particles per unit volume, $n_1F_{l\text{-}c}$, as a function of Φ_c, where n_1 is the number of lamellar membranes per unit volume ($n_1=1.01\times10^7$ for Φ_s=3.1%). The frustration energy increases with the increase of Φ_c and

reaches 10^3-10^4 J/m^3 at $\Phi_c=1.0\%-10\%$. When this additional potential surpasses the free energy difference between the lamellar assembly and the micellar assembly, the morphology transition will take place. Thus, in order to release the frustration due to the restriction of membrane fluctuations, the surfactant assembly transforms the morphology from the two dimensional sheet structure to one dimensional flexible prolate structure which does not have strong confinement effect for colloidal particles.

V. CONCLUSIONS

The depletion interaction is one of the central interactions governing the stability of a binary mixture of hard particles having different sizes or shapes, where the phase behavior is determined by a balance between the mixing entropy and the translational entropy. This concept can be extended to surfactant membrane and polymer mixture systems, where the attractive interlamellar interaction is induced so as to obtain the large free volume for guest polymer chains. In the case of the surfactant membrane and hard particle mixture systems, the free volume of fluctuating membranes is restricted by the presence of colloidal particles, which causes strong repulsive colloid-membrane interaction. Further addition of the colloidal particles brings the lamellar membrane to prolate micelle transition. Thus the surfactant assemblies reduce the entropic frustration by changing the morphology instead of the overlapping of the depletion zone. This may be a unique feature of the surfactant assembly and hard particle mixtures.

ACKNOWLEDGMENTS

This work is supported by KAKENHI (Grant-in-Aid for Scientific Research) on Priority Area "Soft Matter Physics" and Grant-in-Aid Scientific Research (B) (Grant No. 19340118) from the Ministry of Education, Culture, Sports, Science and Technology of Japan. The SANS experiments were done under the approval of the Neutron Scattering Program Advisory Committee.

[1] S. Asakura and F. Oosawa, J. Chem. Phys. **22**, 1255 (1954).
[2] A. Vrij, Pure Appl. Chem. **48**, 471 (1976).
[3] V. J. Anderson and H. N. W. Lekkerkerker, Nature (London) **416**, 811 (2002).
[4] P. B. Warren, J. Phys. I **4**, 237 (1994).
[5] T. Koda, M. Numajiri, and S. Ikeda, J. Phys. Soc. Jpn. **65**, 3551 (1996).
[6] M. Adams, Z. Dogic, S. L. Keller, and S. Fraden, Nature (London) **393**, 349 (1998).
[7] G. H. Koenderink, G. A. Vliegenthart, S. G. J. M. Kluijtmans, A. van Blaaderen, A. P. Philipse, and H. N. W. Lekkerkerker, Langmuir **15**, 4693 (1999).
[8] Z. Dogic, D. Frenkel, and S. Fraden, Phys. Rev. E **62**, 3925 (2000).
[9] K.-H. Lin, J. C. Crocker, A. C. Zeri, and A. G. Yodh, Phys. Rev. Lett. **87**, 088301 (2001).
[10] A. Matsuyama and T. Kato, Eur. Phys. J. E **6**, 15 (2001).
[11] M. Imai, N. Urakami, A. Nakamura, R. Takada, R. Oikawa, and Y. Sano, Langmuir **18**, 9918 (2002).
[12] S. V. Savenko and M. Dijkstra, J. Chem. Phys. **124**, 234902 (2006).
[13] M. Daoud and P. G. de Gennes, J. Phys. (France) **38**, 85 (1977).
[14] J. T. Brooks and M. E. Cates, J. Chem. Phys. **99**, 5467 (1993).
[15] C. Ligoure, G. Bouglet, G. Porte, and O. Diat, J. Phys. II **7**, 473 (1997).
[16] L. Porcar, C. Ligoure, and J. Marignan, J. Phys. II **7**, 493 (1997).
[17] G. Bouglet, C. Ligoure, A.-M. Bellocq, E. Dufoure, and G. Mosser, Phys. Rev. E **57**, 834 (1998).
[18] V. Ponsinet and P. Fabre, J. Phys. II **6**, 955 (1996).
[19] M. Imai, R. Mawatari, K. Nakaya, and S. Komura, Eur. Phys. J. E **13**, 391 (2004).
[20] P. Sens, M. S. Tumor, and P. Pincus, Phys. Rev. E **55**, 4394 (1997).
[21] W. Helfrich, Z. Naturforsch. A **33a**, 305 (1978).
[22] R. Strey, R. Schomäcker, D. Roux, F. Nallet, and U. Olsson, J. Chem. Soc., Faraday Trans. **86**, 2253 (1990).
[23] Y. Ito, M. Imai, and S. Takahashi, Physica B **213–214**, 889 (1995).
[24] S. Okabe, M. Nagao, T. Karino, S. Watanabe, T. Adachi, H. Shimizu, and M. Shibayama, J. Appl. Crystallogr. **38**, 1035 (2005).
[25] A. Caillé, Comptes Rendus des Seances de l'Academie des Science, Serie B: Sciences Physique **274**, 891 (1972).
[26] F. Nallet, D. Roux, C. Quilliet, P. Fabre, and S. T. Milner, J. Phys. II **4**, 1477 (1994).
[27] F. Nallet, R. Laversanne, and D. Roux, J. Phys. II **3**, 487 (1993).
[28] C. J. Glinka, J. M. Rowe, and J. G. LaRock, J. Appl. Crystallogr. **19**, 427 (1986).
[29] T. Masui, M. Imai, K. Nakaya, and T. Taniguchi, J. Chem. Phys. **124**, 074904 (2006).
[30] Y. Suganuma, M. Imai, and K. Nakaya, J. Appl. Crystallogr. **40**, s303 (2007).
[31] M. Kotlarchyk and S.-H. Chen, J. Chem. Phys. **79**, 2461 (1983).
[32] J. B. Hayter and J. Penfold, Colloid Polym. Sci. **261**, 1022 (1983).
[33] J.-P. Hansen and I. R. McDonald, *Theory of Simple Liquids*, 3rd ed. (Academic, Amsterdam, 2006).
[34] S. Shirai, S. Yoshimura, and Y. Einaga, Polym. J. (Tokyo, Jpn.) **38**, 37 (2006).
[35] A. Bernheim-Groswasser, E. Wachtel, and Y. Talmon, Langmuir **16**, 4131 (2000).
[36] M. Imai, Y. Suganuma, K. Nakaya, and S. Komura, J. Phys.: Condens. Matter **17**, S2929 (2005).
[37] H. N. W. Lekkerkerker, W. C.-K. Poon, P. N. Pusey, A. Stroobants, and P. B. Warren, Europhys. Lett. **20**, 559 (1992).
[38] P. G. Bolhuis and H. N. W. Lekkerkerker, Physica A **196**, 369 (1993).
[39] T. Kato, S. Anzai, and T. Seimiya, J. Phys. Chem. **94**, 7255 (1990).